Ultrafast Science
A SCIENCE PARTNER JOURNAL

RESEARCH ARTICLE

External-Magnetic-Field-Free Spintronic Terahertz Strong-Field Emitter

Shaojie Liu[1†], Zejun Ren[2†], Peng Chen[3,4†], Sai Chen[2†], Mingxuan Zhang[2], Zehao Yang[2,5], Deyin Kong[2,5], Jinguang Wang[3], Yifei Li[3], Jinglong Ma[3], Xin Lu[3,4,6], Baolong Zhang[7], Zhongkai Liu[8], Xiufeng Han[3,4], Caihua Wan[3*], Yutong Li[3,6*], Ranjan Singh[7], and Xiaojun Wu[1,2,5,9*]

[1]School of Cyber Science and Technology, Beihang University, Beijing 100191, China. [2]School of Electronic and Information Engineering, Beihang University, Beijing 100083, China. [3]Beijing National Laboratory for Condensed Matter Physics, Institute of Physics, Chinese Academy of Sciences, Beijing 100190, China. [4]Center of Materials Science and Optoelectronics Engineering, University of Chinese Academy of Sciences, Beijing 100049, China. [5]Zhangjiang Laboratory, Shanghai 201204, China. [6]Songshan Lake Materials Laboratory, Dongguan 523808, Guangdong, China. [7]Division of Physics and Applied Physics, School of Physical and Mathematical Sciences, Nanyang Technological University, Singapore 637371, Singapore. [8]School of Physical Science and Technology, ShanghaiTech University, Shanghai 201210, China. [9]Wuhan National Laboratory for Optoelectronics, Huazhong University of Science and Technology, Wuhan 430074, China.

*Address correspondence to: wancaihua@iphy.ac.cn (C.W.); ytli@iphy.ac.cn (Y.L.); xiaojunwu@buaa.edu.cn (X.W.)
†These authors contributed equally to this work.

Citation: Liu S, Ren Z, Chen P, Chen S, Zhang M, Yang Z, Kong D, Wang J, Li Y, Ma J, et al. External-Magnetic-Field-Free Spintronic Terahertz Strong-Field Emitter. *Ultrafast Sci.* 2024;4:Article 0060. https://doi.org/10.34133/ultrafastscience.0060

Submitted 30 November 2023
Accepted 1 March 2024
Published 22 May 2024

Intense terahertz (THz) radiation in free space has immense potential for regulating material state, accelerating electrons, producing biological effects, and so on. However, the high cost and challenges involved in constructing strong-field THz sources have limited their developments, making it difficult for the potential applications of strong-field THz radiation to be widely adopted. Spintronic THz emitters (STEs) with numerous merits such as high efficiency, ultrabroadband, ease of integration, and low cost have become ubiquitous, but the majority of these emitters require stable operation in the presence of external magnets, limiting their applications, particularly in generating strong fields that necessitate large-sized samples. Here, we demonstrate the feasibility of generating strong-field THz radiation in 4-inch antiferromagnetic material–ferromagnetic metal ($IrMn_3$ [2 nm]/$Co_{20}Fe_{60}B_{20}$ [2 nm]/W [2 nm]) without external magnetic field driving. Under the excitation of a Ti:sapphire femtosecond laser amplifier with a 35-fs pulse duration and a 1-kHz repetition rate, we obtain strong-field THz radiation from our STEs with a pulse duration of ~110 fs, and a spectrum covering up to ~10 THz. Further scaling up the pump laser energy up to 55 mJ with a pulse duration of ~20 fs and a repetition rate of 100 Hz provided by the Synergetic Extreme Condition User Facility, the radiated THz electric field strength from the external-magnetic-free 4-inch STEs can exceed 242 kV/cm with a pulse duration of ~230 fs, a spectrum covering up to ~14 THz, and a single pulse energy of 8.6 nJ measured by a calibrated pyroelectric detector. Our demonstrated external-magnetic-field-free high-field STEs have some unique applications such as producing sub-cycle ultrashort strong THz fields in huge size emitters under the excitation of high-energy light sources, accelerating the development of THz science and applications.

Introduction

The emergence of high-energy, strong-field terahertz (THz) light sources has enabled marked advancements in THz scientific and technological frontiers in recent years. In particular, the studies on THz light–matter non-equilibrium interaction [1–4] and THz electron acceleration [5–8] have paved the way for extending electromagnetic wave interaction to the last yet-to-be-explored electromagnetic frequency range. Intense electric fields at the THz frequency range can influence the electric orbitals of materials, while magnetic fields can induce spin processes and create non-equilibrium magnetic structures in quantum states. Furthermore, the different frequencies of THz radiation correlate to distinct lattice vibration modes of quantum materials, which may impact their intrinsic properties through resonant or non-resonant interactions with phonons

[9]. In addition to being useful for many applications requiring high electric and magnetic fields, intense THz is vital for comprehending low-energy elementary excitation around the Fermi energy level, as the energy of THz photons permits the investigation of nonthermal processes of matter. Strong-field THz has therefore been used to engineer the energy band structure in topological insulators [2], investigate the structural phase transition mechanism in quantum materials [10], stimulate the layer coupling modes in 2-dimensional materials [11], and observe the direct coupling of phonon and magnon in antiferromagnetic materials [12].

The robust utilization of strong-field THz spectroscopy for investigating materials is challenged by the requirement of high-stability, high-beam-quality, and high-efficiency THz radiation sources, which imposes limitations on the resonant energies and physical dimensions of materials that can be probed. Among the most promising systems are ultrashort THz pulses, which have exceptional sub-cycle temporal waveforms and exceedingly strong peak electric fields, leading to an unprecedented non-equilibrium state in the matter. However, generating stable and high-quality strong-field THz radiations of extremely short durations and ultrabroadband frequency ranges present considerable challenges, thereby making it difficult to realize practical applications.

Femtosecond laser-driven tabletop intense THz sources have demonstrated their capacity to meet the aforementioned requirements [13–18], particularly solid-state strong-field THz emitters based on lithium niobate materials and organic crystals [19–22]. Organic material-based THz emitters suffer from a basic limitation, as they lack inherent high stability, rendering them prone to damage and deliquescence. Furthermore, to produce THz radiation efficiently from organic crystals, wavelengths longer than 1 μm need to be used. Nonetheless, much longer pump wavelengths have been explored less extensively and efficiently than Ti:sapphire lasers. Over the years, strong-field THz generators that rely on lithium niobate crystals have made substantial advancements by utilizing the tilted pulse front technique to tackle the issue of phase mismatching. Although these THz sources are widely used, they are still subject to certain shortcomings, such as having a complicated radiation process, needing a bulky tilted pulse front optical system, demanding cryogenic cooling of crystals in a vacuum space, and lacking polarization tunability. Thus, the development of stable THz emitters with high peak fields, short pulse duration, and adaptable polarization control is still a crucial challenge.

The emission of THz waves through spintronics, which is an alternate source of femtosecond laser-driven THz radiation, is a spin current conversion technique that can generate THz waves with high efficiency, great beam quality, and exceptional stability [23–25]. This method can be scaled up by several orders of magnitude to produce ultrashort THz transients [26–30]. Due to the capability of constructing vast nanofilms and heterostructures, it is possible to efficiently manufacture strong-field THz beams utilizing conventional coating technology that is robust and magnetron sputtering production that is simple. From large-area Pt/$Co_{20}Fe_{60}B_{20}$/W samples, Seifert et al. [31] generated a THz pulse with peak fields of 300 kV/cm, and Rouzegar et al. [32] enhanced the performance to 1.5 MV/cm by optimizing the structures via both photonic and thermal management. However, conventional spintronic THz emitters (STEs) require the use of external magnets, which hinders the development of STE samples with enormous dimensions to produce strong-field THz radiation.

Using a Ti:sapphire femtosecond laser amplifier, we have demonstrated that antiferromagnetic-ferromagnetic heterostructures, with an area of 4 inches, can produce high-performance, strong-field THz pulses without the aid of external magnetic fields (EMF). This THz generator has the potential for vast applications due to its extremely short pulse length of 110 fs and ultrabroadband radiation frequencies of more than 10 THz. Upon the excitation of a high-energy light source of 55-mJ pumping, a 242-kV/cm THz field strength with a single pulse energy of 8.6 nJ is achieved. This is the first STE that can create strong-field THz radiation without EMF. With its remarkable radiation performance, stability, and affordability, it will be widely used in the THz field.

Materials and Methods

$IrMn_3$ (2 nm)/$Co_{20}Fe_{60}B_{20}$ (2 nm)/W (2 nm) heterostructures for strong-field THz emission were manufactured at room temperature by magnetron sputtering on 1-mm-thick, 4-inch-diameter, double-polished fused quartz plates, as shown in the inset of Fig. 1A. The base pressure of the chamber was less than 2×10^{-8} Torr when a 180-Oe in-plane EMF was used to induce the exchange bias or coupling.

Figure 1A depicts the experimental diagram. To generate strong-field THz pulses, a Ti:sapphire laser amplifier produces femtosecond laser pulses with a pulse duration of 35 fs, a repetition rate of 1 kHz, a maximum pump energy of 4 mJ, and a central wavelength of 800 nm is used. Before beaming onto the 4-inch heterostructures, a 10-mm-diameter femtosecond pump beam is directed onto a 10× telescope with a concave mirror ($f = -50$ mm) and a convex mirror ($f = 500$ mm). In a 0.1-mm-thick ZnTe detection crystal, the electric field temporal waveform of the transmitted THz is captured using a standard electro-optic (EO) sampling method. The Supplementary Materials contain additional information regarding the experimental apparatus.

To effectively radiate strong-field THz radiation from the STE without EMF, as depicted in Fig. 1B, the $Co_{20}Fe_{60}B_{20}$ layer (ferromagnetic metal [FM]) between $IrMn_3$ (antiferromagnetic metal [AFM]) and W (heavy metal [HM]) is initially "magnetized" in-plane via the exchange coupling effect between AFM and FM layers. Then, when femtosecond laser pulses are absorbed by the magnetized $Co_{20}Fe_{60}B_{20}$ FM layer, spin-up and spin-down electrons will be excited above the Fermi energy level. Because they have different densities and mobilities, a longitudinal spin-polarized current $\vec{J}_s$ is produced. It includes both forward- and backward-flowing spin current ($\vec{J}_{s-W}$ and $\vec{J}_{s-IrMn_3}$) components concerning the interfaces of $Co_{20}Fe_{60}B_{20}$/W and $IrMn_3$/$Co_{20}Fe_{60}B_{20}$, respectively. At the interface, spin-orbit field causes spin-up and spin-down electrons to deflect in opposite directions and subsequently convert spin currents into a transverse in-plane charge current ($\vec{J}_{c-IrMn_3}$ and $\vec{J}_{c-W}$) via the inverse spin Hall effect (ISHE), where γ_{IrMn3} and γ_W are the spin Hall angles for $IrMn_3$ and W, respectively [23,33]. When $IrMn_3$ and W have opposite spin Hall angles, the charge currents, which are converted from the backward and forward spin currents, have the same direction. In addition, the STE has a total thickness of only 6 nm, which is insufficient for separating the 2-THz electric fields in time domain. Consequently, the

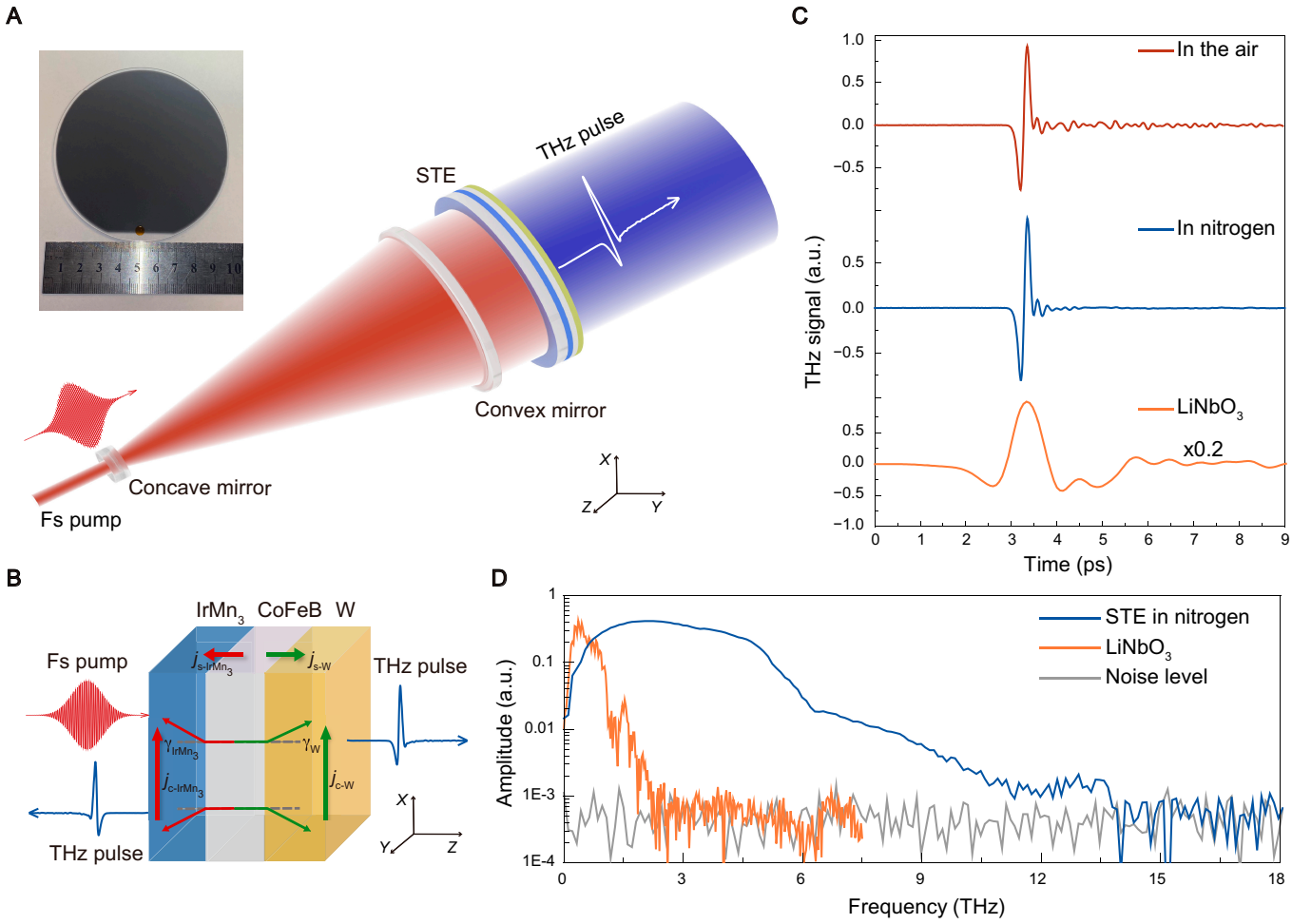

Fig. 1. Ultrabroadband strong-field THz radiation from 4-inch $IrMn_3$ (2 nm)/$Co_{20}Fe_{60}B_{20}$ (2 nm)/W (2 nm) without EMF. (A) Illustration of the ultrabroadband strong-field THz emission principle. The inserted photograph is the 4-inch strong-field STE. (B) Principle of operation. (C) Recorded typical THz transients radiated from the AFM/FM/HM heterostructure in the air (red line) and in nitrogen (blue line) as well as that from the lithium niobate crystal via tilted pulse front technique (orange line). (D) Corresponding Fourier transform spectra of the STE THz transients detected in nitrogen and the THz transients from the lithium niobate crystal in (C); the gray line represents noise level.

radiated THz transients can be amplified and effectively augmented via coherent superposition, as shown in Eq. 1. Here, $\vec{m}$ denotes the magnetization direction of the $Co_{20}Fe_{60}B_{20}$ layer.

$$\begin{aligned}\vec{E}_{THz} &\propto \vec{J}_c = \vec{J}_{c-\mathrm{IrMn_3}} + \vec{J}_{c-\mathrm{W}} \\ &= \gamma_{\mathrm{IrMn_3}} \cdot \left(\vec{J}_{s-\mathrm{IrMn_3}} \times \vec{m}\right) + \gamma_W \cdot \left(\vec{J}_{s-\mathrm{W}} \times \vec{m}\right)\end{aligned} \quad (1)$$

This equation depicts the relationship between the amplitude of THz radiation emitted and its polarization state, which is determined by the spin-polarized current. The radiated THz pulses should be linearly polarized and perpendicular to the converted charge current.

Results and Discussion

Ultrabroadband strong-field THz radiation

According to the design strategy outlined in Fig. 1C, our 4-inch STE sample emits powerful THz radiation without EMF. Under the 4-mJ pump energy, the sub-cycle THz electro-optic signals of the heterostructures measured in both nitrogen and ambient conditions have pulse widths of approximately ~110 fs (full width at half maximum [FWHM]). In comparison and to assess the STE performance, a THz electric signal is generated from a lithium niobate crystal via the tilted pulse front technique with the same detecting conditions and 2.5-mJ pump energy. The THz electric peak amplitude from the STE is approximately one-fifth that from the lithium niobate crystal. However, the Fourier transform spectrum of the STE has a much wider bandwidth, extending up to 10 THz with a peak frequency of 2 THz, especially when there is no water vapor interference, as shown in Fig. 1D. Since the strong-field THz emitter based on spintronics lacks phonon absorption, the generated THz pulse duration depends primarily on the pump laser pulse width, making it ideal for studies requiring low photon energies and ultrafast time resolution for THz field-controlled light–matter interaction studies.

Magnetic-field-free THz radiation mechanism

In Fig. 2, we give a more comprehensive experimental investigation. It is important to note that the femtosecond laser-induced THz radiation with a strong field is polarized perpendicularly to the direction of spin pinning (Y-axis). This indicates that the exchange bias direction (Y-axis) is vertical to the polarization

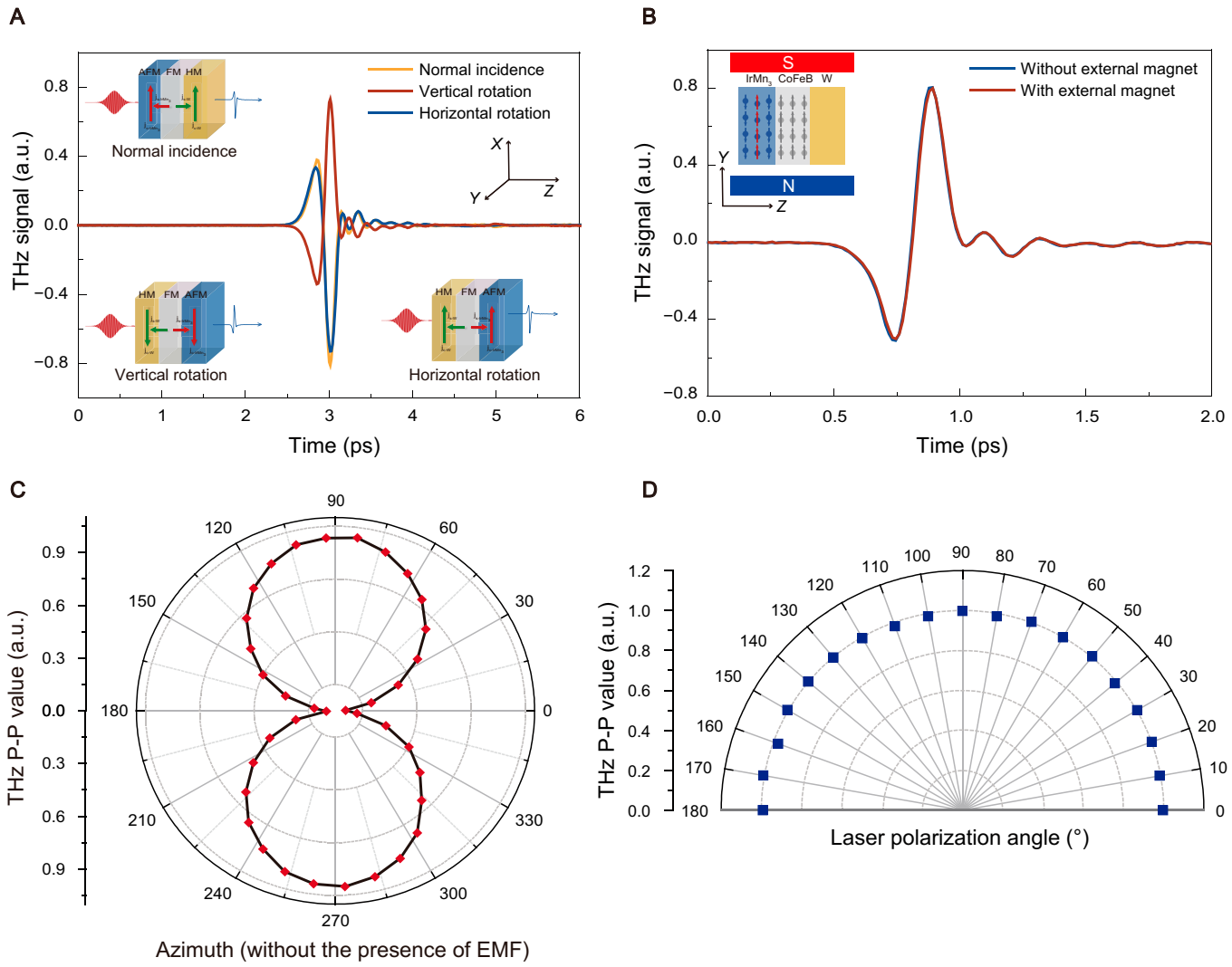

Fig. 2. Strong-field THz polarity and polarization control. (A) Radiated THz phase reversal via flipping the femtosecond pump incident facet along the spin pinning direction. (B) THz radiation intensity under the condition of with or without EMF. (C) THz P-P value as a function of the rotation sample azimuthal angles. THz P-P value: THz peak-to-peak value. (D) Femtosecond pump polarization independence on the radiated THz yields.

direction (*X*-axis) of the THz waves when no magnetic fields are present. Thus, flipping the pinning axis allows us to reverse the THz polarity with ease. In Fig. 2A, the THz waveforms are presented for horizontal and vertical rotations relative to the normal incidence scenario, suggesting that the exchange coupling effect results in symmetry-breaking properties of THz radiation. This characteristic is qualitatively consistent with Eq. 1, as the linearly polarized THz waves originate from spin-to-charge converted currents produced by $IrMn_3$ pinned $Co_{20}Fe_{60}B_{20}$ in the absence of EMF.

In addition to the ability to reverse THz polarity, there is a high demand for THz pulses with high intensity and beam quality for practical applications. To determine the quality of the STE, a 20-mT magnetic field was administered externally. If the spin pinning effect at the interface of AFM and FM layers was not uniform or strong enough to saturate the magnetization, an increase in THz emission would be observed when the external magnetization direction was parallel to the spin pinning direction, according to our hypothesis. As depicted in Fig. 2B, the intensity of THz radiation was nearly identical in the presence and absence of EMF. Our experimental findings corroborate that the exchange coupling effect between the AFM and FM layers is sufficiently strong and that this magnetic-field-free AFM/FM/HM heterostructure is ideal for emitting high-field THz pulses.

We rotate the azimuthal angle of the STE by 360° and measure the peak-to-peak (P-P) values of the THz electric field to expand the range of the linearly polarized THz pulses. As demonstrated in Fig. 2C, the radiation pattern corresponds to Eq. 1. In addition, as shown in Fig. 2D, the pump polarization independence behavior demonstrates that neither the absorption of pump light by $Co_{20}Fe_{60}B_{20}$ nor the exchange coupling effect is chirality-dependent. The radiation pattern from the 4-inch sample was preferable to that of the 1-mm sample, according to our previous investigation [23].

STE damage threshold characterization via laser THz emission spectroscopy

So far, our research has demonstrated the generation of strong-field THz radiation with ultrabroadband using AFM/FM/HM

heterostructures, which have the potential to control the radiation polarization states in various ways. There is a high demand for ultrashort THz pulses with strengths exceeding 200 kV/cm, specifically for achieving non-equilibrium THz electromagnetic field-driven quantum phase manipulation [1,3,4,10,11,34]. Figure 3A depicts data revealing a positive relationship between the P-P value of strong-field THz radiation and the pump fluence, suggesting that boosting the pump laser energy is an easy and efficient method to enhance the THz field strength. Although highly efficient THz waves are generated due to strong absorption leading to high current density, the nanometer-thick AFM/FM/HM heterostructures comprising the device make them highly susceptible to heat damage. Therefore, it is crucial to determine the damage threshold of surface-terminated semiconductor electrodes subjected to ultra-intense and ultrashort femtosecond laser pulses to address this issue. The sensitivity of laser THz emission spectroscopy enables utilizing THz emission spectroscopy data directly to derive the sample damage threshold [35–37].

As shown in Fig. 3A, since the highest pump fluence of 0.05 mJ/cm^2 does not produce radiation saturation or a decrease, there is no need to increase the size of the pump beam for this experiment. To boost the pump fluence, the 7-mm (full width) spot of the femtosecond laser amplifier is used, and then the THz electric field signal is analyzed through EO sampling. The material surface morphology is also analyzed using a camera. Figure 3B displays the THz radiation transients for various pump fluences. The graph demonstrates that the THz radiation signal initially increases, followed by a gradual decrease as the pump fluence continues to rise. To gain a clearer idea of the damage threshold, the P-P values of the emitted THz electric field are extracted at various pump fluences, and their correlation is shown in Fig. 3C. For the smallest pump spot, the experimental threshold measurement indicates that the strongest THz radiation is detected at a pump fluence of 1.2 mJ/cm^2. Clearly, the sample was on the brink of damage, as shown in the photographs of the sample surface topography included here. An increase in the pump fluence leads to a marked drop

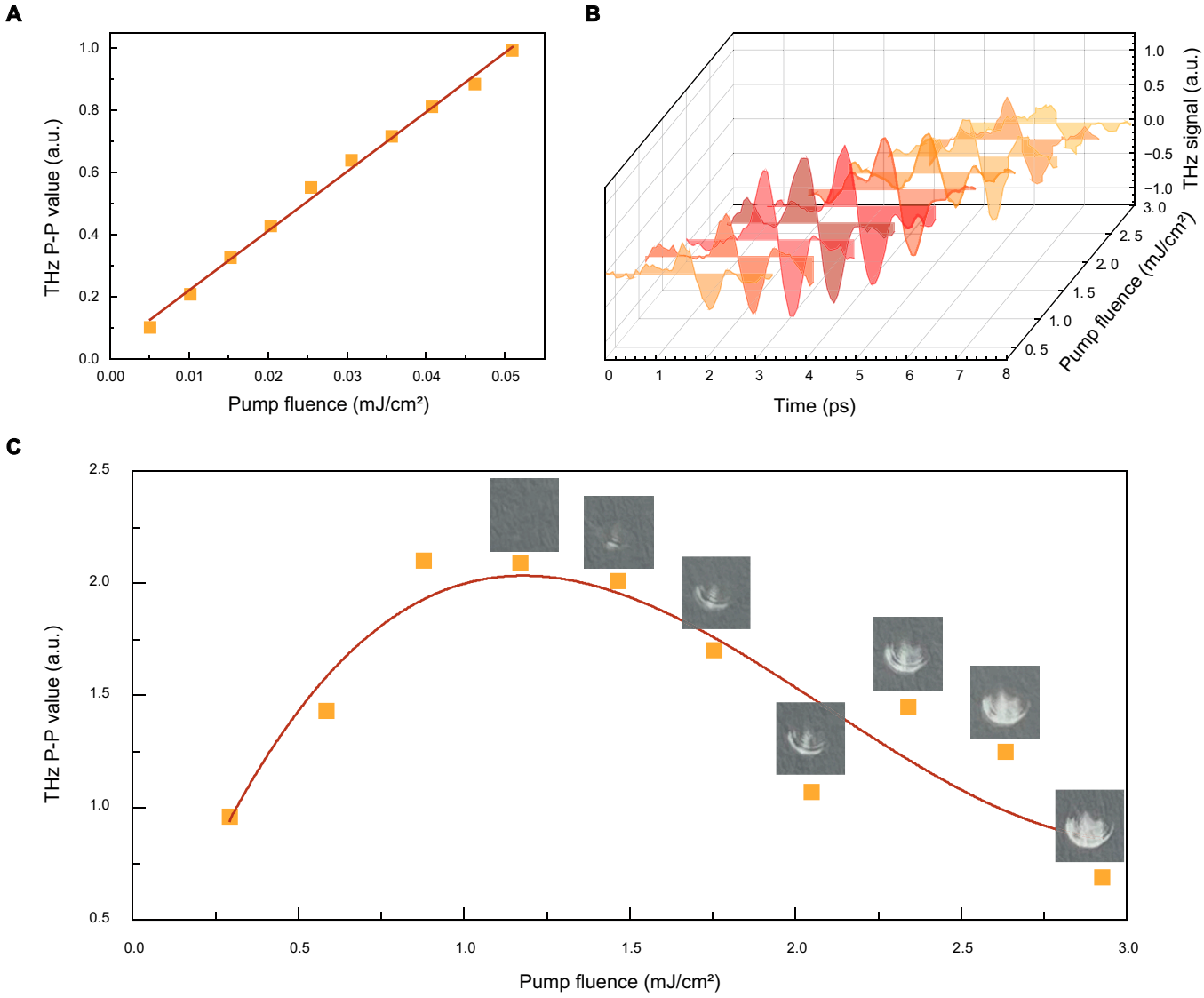

Fig. 3. STE damage threshold characterization. (A) The P-P value of strong-field THz as a function of the pump fluence. (B) THz transients are under various pump fluences. (C) THz electric field P-P values under different pump fluences. The insets show the sample surface morphology under the corresponding pump fluence.

in THz intensity, and the sample surface topography reveals distinct areas of ablation. The photographs of the sample morphology indicate an increase in white areas, signifying the gradual dissolution of the heterostructure nanofilms on the fused quartz substrate within the pump light spot area, resulting in an increasing amount of white substrate. In this study, laser THz emission technology is used in combination with a cost-effective camera to monitor experiments and determine the damage threshold of $IrMn_3/Co_{20}Fe_{60}B_{20}/W$ for femtosecond pulses with a central wavelength of 800 nm, a pulse width of 35 fs, and a repetition rate of 1 kHz. The results show that the damage threshold is 1.2 mJ/cm^2. The sample damage thresholds could differ at different wavelengths, pulse widths, and repetition rates. However, the proposed methodology can be a workable means of measurement. Based on the determined damage threshold of 1.2 mJ/cm^2, the maximum THz radiation electric field from the 4-inch strong-field STE without external magnets would exceed 200 kV/cm when computed based on the trend shown in Fig. 3A. However, STE operating principles are more transparent, and it is less expensive, producing shorter THz pulses with a broader spectrum, competing with the strong-field THz radiation of lithium niobates in various ways. The STEs are applicable to any wavelength and has more stable benefits than organic crystals and plasma THz strong sources. Increasing the field strength of STE is also possible by preparing larger samples and loading more laser pump energy. Due to widespread availability of femtosecond laser amplifiers with higher pump energy, preparing 6- or even 8-inch samples is entirely feasible. Consequently, the proposed strong-field THz emission technique without an EMF and the derived laser THz emission threshold measurement approach lay the foundation for creating powerful THz sources using ultrafast spintronics.

Two-dimensional imaging of THz beams by a CCD camera

Besides the field strength where the strong-field THz applications matter, the quality of a THz beam is also an important factor for practical purposes in addition to its magnitude. To evaluate the profile of the focused THz beam, an experimental apparatus comprising a digital charge coupled device (CCD) camera and a polarization beam splitter was utilized, as illustrated in Fig. 4A. A 4-inch STE generated a strong-field THz that caused birefringence in the 1-mm-thick ZnTe detection crystal, resulting in the probing beam becoming elliptical. The captured optical image shown in Fig. 4B was analyzed to determine the peak field distribution of the THz beam at the focal point. The concentrated THz beam exhibited a comparatively smaller diameter than that achieved through the tilted pulse front technique in lithium niobate crystals. The superior focusing ability of STEs stems from their higher peak frequency in the strong-field THz they generate.

Obtaining strong-field THz radiation

To generate high-field THz radiation exceeding 200 kV/cm, we employed a laser facility of the Synergetic Extreme Condition User Facility (SECUF), which delivers a maximum pulse energy of 55 mJ at the sample position with a central wavelength of 800 nm, a pulse duration of 20 fs, and a repetition rate of 100 Hz. As depicted in Fig. 5A, the femtosecond laser pump beam is first expanded to 4 inches in the beam diameter through a telescope constructed by 2 off-axis parabolic mirrors (OAPs) in a vacuum chamber. The expanded collimated beam is then reflected by a reflection mirror and then illuminates onto the STE sample for the generation of high-field THz pulses. The radiated THz wave is collected by the OAP 3 with a 4-inch focal length and focused onto a GaP detection crystal with a thickness of 50 μm. For the EO sampling measurement, the probing beam is split from the pump beam with a small (1/2 inch) elliptical mirror. After going through a reflection mirror and a translation stage, the probing beam and the THz pulses illuminate onto the detection crystal simultaneously in space and time.

Figure 5B depicts the typical THz temporal waveforms generated from $IrMn_3/Co_{20}Fe_{60}B_{20}/W$ and its corresponding spectrum is plotted in Fig. 5C. It is found that the radiated THz electric field has a pulse duration of ~230 fs (FWHM) with a peak frequency at ~1 THz and a spectrum exceeding 14 THz under the excitation of 20-fs pulses. We employed a pyroelectric detector (Gentec SDX-1152) to measure the THz single-pulse energy. As summarized in Fig. 5D, the detected THz energy reflects a linear dependence on the pump fluence. Under a

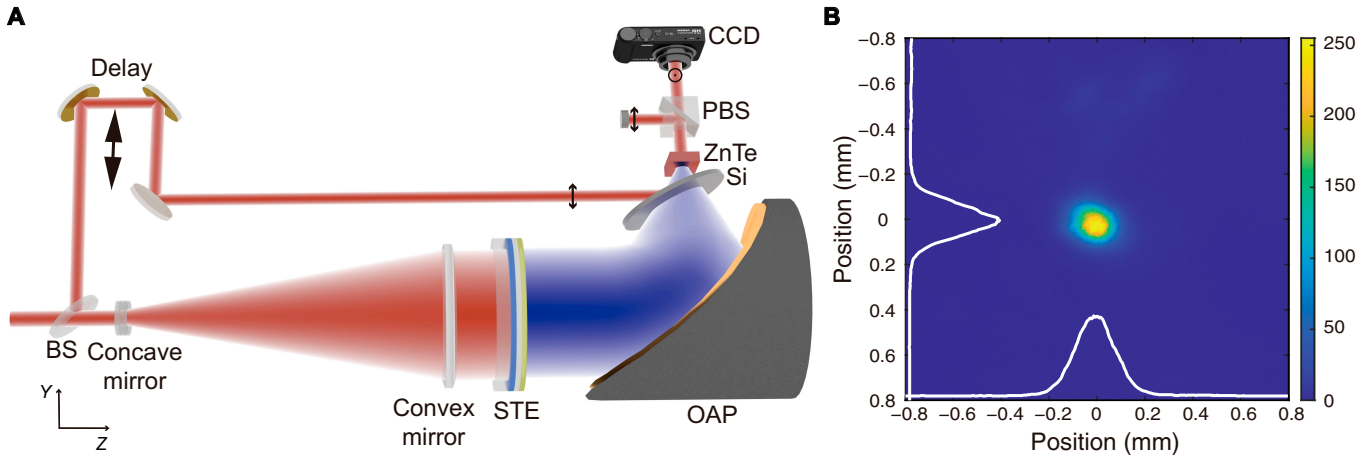

Fig. 4. Focused THz beam profile. (A) Schematic diagram of a THz beam captured by the CCD camera using EO sampling. BS: beam splitter; OAP: off-axis parabolic mirror; Si: high-resistivity silicon wafer; PBS: polarization beam splitter. (B) Focused THz beam profile with a diameter of ~0.175 mm (1/e) measured at the focus of the OAP.

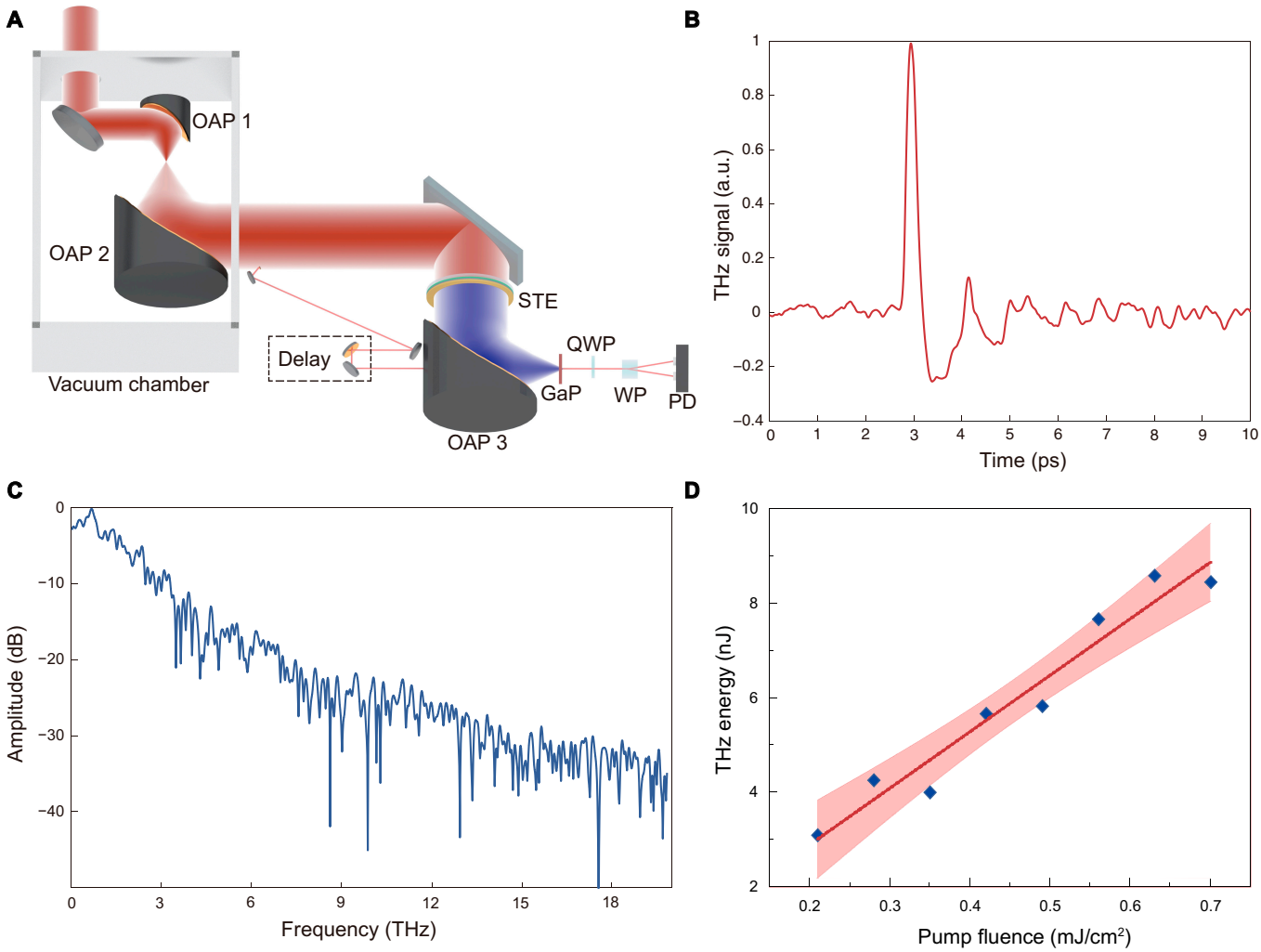

Fig. 5. Exceeding 242-kV/cm high-field THz generation from STEs without EMF under the excitation of ~55-mJ laser pulses. (A) Experimental setup. OAP: off-axis parabolic mirrors; QWP: quarter-wave plate; WP: wollaston prism; BD: balance detector. (B) Typical THz temporal waveform from $IrMn_3/Co_{20}Fe_{60}B_{20}$/W under the excitation of 20-fs laser pulses, and (C) its corresponding spectrum. (D) The THz energy as a function of the laser pump fluence. The red line is a linear fit and the shaded area is the 95% confidence band.

photo-excitation of 0.7 mJ/cm^2 (much lower than the damage threshold of 1.2 mJ/cm^2 obtained before), the detected THz single pulse energy is 8.6 nJ with a focused THz electric field of ~242 kV/cm (see more details of the field strength calculation in the Supplementary Materials). At present, the electric field is constrained by the diffraction limitation, but this can be enhanced by employing a parabolic mirror with a shorter focal length or a larger aperture. Moreover, the radiation is not saturated, while the sample is far from damage, implying that it can generate higher field THz waves with higher pump energy.

Conclusion

In conclusion, the study culminates in the successful fabrication of a 4-inch STE comprising $IrMn_3$ (2 nm)/$Co_{20}Fe_{60}B_{20}$ (2 nm)/ W (2 nm) without the use of an EMF. The results demonstrate the ability of STE to generate a THz field with a peak intensity of up to 242 kV/cm. The THz radiation is emitted due to the exchange coupling effect and the inverse spin Hall effect. The STE with a diameter of 4 inches exhibits a high sensitivity to femtosecond laser pulses. Moreover, the polarization of THz radiation can be manipulated by varying the azimuthal angle of the STE. It is expected that the absence of a magnetic field in the ultrashort strong-field STE would stimulate the implementation of more pragmatic applications in the fields of nonlinear THz optics, THz biological effects, and strong-filed THz science and applications.

Acknowledgments

We would like to thank the ultrafast x-ray dynamic experimental station under the Synergetic Extreme Condition User Facility (SECUF) in China.
Funding: This work is supported by the National Key R&D Program of China (2022YFA1604402), the National Natural Science Foundation of China (11827807, 92250307, and 62005140), and the Open Project Program of Wuhan National Laboratory for Optoelectronics No. 2022WNLOKF006.
Author contributions: X.W. conceived and coordinated the strong-field spintronic THz generation and application project. X.W., S.L., M.Z., and D.K. designed the experimental setup and carried out the experiments. P.C., and C.W. fabricated the 4-inch antiferromagnetic–ferromagnetic heterostructures. S.L., Z.R., Z.Y., D.K., J.W., Yifei Li, J.M., X.L., and

Yutong Li designed the high-field THz experimental setup and carried out the high-field THz experiments by SECUF. X.W., S.L., S.C., M.Z., B.Z., and R.S. wrote the manuscript with input from all authors.
Competing interests: The authors declare that they have no competing interests.

Data Availability

The data that support the findings of this study are available from the corresponding author upon reasonable request.

Supplementary Materials

Figs. S1 to S4

References

1. Dong T, Zhang SJ, Wang NL. Recent development of ultrafast optical characterizations for quantum materials. *Adv Mater*. 2022;35(27):2110068.
2. Reimann J, Schlauderer S, Schmid CP, Langer F, Baierl S, Kokh KA, Tereshchenko OE, Kimura A, Lange C, Guedde J, et al. Subcycle observation of lightwave-driven Dirac currents in a topological surface band. *Nature*. 2018;562(7727):396–400.
3. Bao C, Tang P, Sun D, Zhou S. Light-induced emergent phenomena in 2D materials and topological materials. *Nat Rev Phys*. 2022;4(1):33–48.
4. Sekiguchi F, Hirori H, Yumoto G, Shimazaki A, Nakamura T, Wakamiya A, Kanemitsu Y. Enhancing the hot-phonon bottleneck effect in a metal halide perovskite by terahertz phonon excitation. *Phys Rev Lett*. 2021;126(7):077401.
5. Filippetto D, Musumeci P, Li RK, Siwick BJ, Otto MR, Centurion M, Nunes JPF. Ultrafast electron diffraction: Visualizing dynamic states of matter. *Rev Mod Phys*. 2022;94(4):045004.
6. Tang H, Zhao L, Zhu P, Zou X, Qi J, Cheng Y, Qiu J, Hu X, Song W, Xiang D, et al. Stable and scalable multistage terahertz-driven particle accelerator. *Phys Rev Lett*. 2021;127(7):074801.
7. Xu H, Yan L, Du Y, Huang W, Tian Q, Li R, Liang Y, Gu S, Shi J, Tang C. Cascaded high-gradient terahertz-driven acceleration of relativistic electron beams. *Nat Photonics*. 2021;15(6):426–430.
8. Hibberd MT, Healy AL, Lake DS, Georgiadis V, Smith EJH, Finlay OJ, Pacey TH, Jones JK, Saveliev Y, Walsh DA, et al. Acceleration of relativistic beams using laser-generated terahertz pulses. *Nat Photonics*. 2020;14(12):755–759.
9. Kampfrath T, Tanaka K, Nelson KA. Resonant and nonresonant control over matter and light by intense terahertz transients. *Nat Photonics*. 2013;7(9):680–690.
10. Li X, Qiu T, Zhang JH, Baldini E, Lu J, Rappe AM, Nelson KA. Terahertz field-induced ferroelectricity in quantum paraelectric $SrTiO_3$. *Science*. 2019;364(6445):1079–1082.
11. Sie EJ, Nyby CM, Pemmaraju CD, Park SJ, Shen X, Yang J, Hoffmann MC, Ofori-Okai BK, Li R, Reid AH, et al. An ultrafast symmetry switch in a Weyl semimetal. *Nature*. 2019;565(7737):61–66.
12. Mashkovich EA, Grishunin KA, Dubrovin RM, Zvezdin AK, Pisarev RV, Kimel AV. Terahertz light-driven coupling of antiferromagnetic spins to lattice. *Science*. 2021;374(6575):1608–1611.
13. Liao G, Liu H, Scott GG, Zhang Y, Zhu B, Zhang Z, Li Y, Armstrong C, Zemaityte E, Bradford P, et al. Towards terawatt-scale spectrally tunable terahertz pulses via relativistic laser-foil interactions. *Phys Rev X*. 2020;10(3):031062.
14. Jia W, Liu M, Lu Y, Feng X, Wang Q, Zhang X, Ni Y, Hu F, Gong M, Xu X, et al. Broadband terahertz wave generation from an epsilon-near-zero material. *Light Sci Appl*. 2021;10(1):11.
15. Koulouklidis AD, Gollner C, Shumakova V, Fedorov VY, Pugzlys A, Baltuska A, Tzortzakis S. Observation of extremely efficient terahertz generation from mid-infrared two-color laser filaments. *Nat Commun*. 2020;11(1):292.
16. Yiwen E, Zhang L, Tcypkin A, Kozlov S, Zhang C, Zhang X-C. Broadband THz sources from gases to liquids. *Ultrafast Sci*. 2021;2021:9892763.
17. Tian Y, Liu J, Bai Y, Zhou S, Sun H, Liu W, Zhao J, Li R, Xu Z. Femtosecond-laser-driven wire-guided helical undulator for intense terahertz radiation. *Nat Photonics*. 2017;11(4):242–246.
18. Dey I, Jana K, Fedorov VY, Koulouklidis AD, Mondal A, Shaikh M, Sarkar D, Lad AD, Tzortzakis S, Couairon A, et al. Highly efficient broadband terahertz generation from ultrashort laser filamentation in liquids. *Nat Commun*. 2017;8(1):1184.
19. Zhang B, Ma Z, Ma J, Wu X, Ouyang C, Kong D, Hong T, Wang X, Yang P, Chen L, et al. 1.4-mJ high energy terahertz radiation from lithium niobates. *Laser Photonics Rev*. 2021;15(3):2000295.
20. Guiramand L, Nkeck JE, Ropagnol X, Ozaki T, Blanchard F. Near-optimal intense and powerful terahertz source by optical rectification in lithium niobate crystal. *Photonics Res*. 2022;10(2):340–346.
21. Vicario C, Ovchinnikov AV, Ashitkov SI, Agranat MB, Fortov VE, Hauri CP. Generation of 0.9-mJ THz pulses in DSTMS pumped by a $Cr:Mg_2SiO_4$ laser. *Opt Lett*. 2014;39(23):6632–6635.
22. Wu X. Extreme THz radiation from lithium niobite materials. *Chin Phys Lett*. 2023;40(5):54001.
23. Wu X, Wang H, Liu H, Wang Y, Chen X, Chen P, Li P, Han X, Miao J, Yu H, et al. Antiferromagnetic-ferromagnetic heterostructure-based field-free terahertz emitters. *Adv Mater*. 2022;34(42):2204373.
24. Seifert T, Jaiswal S, Martens U, Hannegan J, Braun L, Maldonado P, Freimuth F, Kronenberg A, Henrizi J, Radu I, et al. Efficient metallic spintronic emitters of ultrabroadband terahertz radiation. *Nat Photonics*. 2016;10(7):483–488.
25. Gueckstock O, Nadvornik L, Gradhand M, Seifert TS, Bierhance G, Rouzegar R, Wolf M, Vafaee M, Cramer J, Syskaki MA, et al. Terahertz spin-to-charge conversion by interfacial skew scattering in metallic bilayers. *Adv Mater*. 2021;33(9):2006281.
26. Huisman TJ, Mikhaylovskiy RV, Costa JD, Freimuth F, Paz E, Ventura J, Freitas PP, Bluegel S, Mokrousov Y, Rasing T, et al. Femtosecond control of electric currents in metallic ferromagnetic heterostructures. *Nat Nanotechnol*. 2016;11(5):455–458.
27. Wu Y, Elyasi M, Qiu X, Chen M, Liu Y, Ke L, Yang H. High-performance THz emitters based on ferromagnetic/nonmagnetic heterostructures. *Adv Mater*. 2017;29(4):1603031.

28. Zhou C, Liu YP, Wang Z, Ma SJ, Jia MW, Wu RQ, Zhou L, Zhang W, Liu MK, Wu YZ, et al. Broadband terahertz generation via the interface inverse Rashba-Edelstein effect. *Phys Rev Lett*. 2018;121(8):086801.
29. Gao Y, Kaushik S, Philip EJ, Li Z, Qin Y, Liu YP, Zhang WL, Su YL, Chen X, Weng H, et al. Chiral terahertz wave emission from the Weyl semimetal TaAs. *Nat Commun*. 2020;11(1):720.
30. Tong M, Hu Y, Wang Z, Zhou T, Xie X, Cheng X, Jiang T. Enhanced terahertz radiation by efficient spin-to-charge conversion in Rashba-mediated Dirac surface states. *Nano Lett*. 2021;21(1):60–67.
31. Seifert T, Jaiswal S, Sajadi M, Jakob G, Winnerl S, Wolf M, Klaeui M, Kampfrath T. Ultrabroadband single-cycle terahertz pulses with peak fields of 300 kV/cm from a metallic spintronic emitter. *Appl Phys Lett*. 2017;110(25):252402.
32. Rouzegar R, Chekhov AL, Behovits Y, Serrano BR, Syskaki MA, Lambert CH, Engel D, Martens U, Münzenberg M, Wolf M, et al. Broadband spintronic terahertz source with peak electric fields exceeding 1.5 MV/cm. *Phys. Rev. Appl.* 2023;19(3): 034018.
33. Jin Z, Peng Y, Ni Y, Wu G, Ji B, Wu X, Zhang Z, Ma G, Zhang C, Chen L, et al. Cascaded amplification and manipulation of terahertz emission by flexible spintronic heterostructures. *Laser Photonics Rev*. 2022;16(9):2100688.
34. Zhou J, Xu H, Shi Y, Li J. Terahertz driven reversible topological phase transition of monolayer transition metal dichalcogenides. *Adv Sci*. 2021;8(12):2003832.
35. Cocker TL, Jelic V, Hillenbrand R, Hegmann FA. Nanoscale terahertz scanning probe microscopy. *Nat Photonics*. 2021;15(8):558–569.
36. Plankl M, Faria Junior PE, Mooshammer F, Siday T, Zizlsperger M, Sandner F, Schiegl F, Maier S, Huber MA, Gmitra M, et al. Subcycle contact-free nanoscopy of ultrafast interlayer transport in atomically thin heterostructures. *Nat Photonics*. 2021;15(8):594–600.
37. Jacobs KJP, Murakami H, Murakami F, Serita K, Beyne E, Tonouchi M. Characterization of through-silicon vias using laser terahertz emission microscopy. *Nat Electron*. 2021;4(3):202–207.